



Synthesis, characterization, and adsorption performance of Pb(II)-imprinted polymer in nano-TiO₂ matrix

LI Chunxiang, GAO Jie, PAN Jianming, ZHANG Zulei, YAN Yongsheng*

School of Chemistry and Chemical Engineering, Jiangsu University, Zhenjiang 212013, China. E-mail: cicity@hotmail.com

Received 24 February 2009; revised 25 May 2009; accepted 27 May 2009

Abstract

Surface ion-imprinted in combination with sol-gel process was applied to synthesis a new Pb(II)-imprinted polymer for selective separation and enrichment of trace Pb(II) from aqueous solution. The prepared material was characterized by using the infrared spectra, X-ray diffractometer, and scanning electron microscopy. The batch experiments were conducted to study the optimal adsorption condition of adsorption trace Pb(II) from aqueous solutions on Pb(II)-imprinted polymer. The equilibrium was achieved in approximately 4.0 h, and the experimental kinetic data were fitted the pseudo second-order model better. The maximum adsorption capacity was 22.7 mg/g, and the Langmuir equation fitted the adsorption isotherm data. The results of selectivity experiment showed that selectively adsorbed rate of Pb(II) on Pb(II)-imprinted polymer was higher than all other studied ions. Desorption conditions of the adsorbed Pb(II) from the Pb(II)-imprinted polymer were also studied in batch experiments. The prepared Pb(II)-imprinted polymer was shown to be promising for the separation and enrichment of trace Pb(II) from water samples. The adsorption and desorption mechanisms were proposed.

Key words: Pb(II); ion-imprinted; sol-gel; adsorption; selective

DOI: 10.1016/S1001-0742(08)62479-1

Introduction

Modern medicine confirms that lead and its compounds are hazardous to people's nerve, blood, digestion, cardiovascular and other endocrine system. Furthermore unlike organic compounds, lead is non-biodegradable, which facilely accumulates in soils and waters. It is well known that lead ions in real water samples are trace levels. Therefore, different approaches have been reported to pre-concentration trace lead ions from aqueous solutions such as liquid-liquid extraction (Anthemidis, 2008), co-precipitation (Tuzena *et al.*, 2008) and solid-phase extraction (Prasad *et al.*, 2006). Because the heavy-metal ions are co-existence in industrial wastewater and other aqueous solutions, selective separation and enrichment a certain kind of heavy metal ions from aqueous solutions becomes necessary.

Molecular imprinting is a method that enables the formation of tailor-made recognition materials by co-polymerizing suitable monomers in the presence of a desired print molecule (Yilmaz *et al.*, 2002). Recently, there are some reports on the application of imprinted technique for separation and enrichment of heavy metal ions (Birlik *et al.*, 2007; Baghel *et al.*, 2007). Among present ion-imprinted technologies, imprinting a matrix with binding sites situated at the surface has many advan-

tages including: the sites are more accessible, mass transfer is faster, and the binding kinetics is faster (Yang *et al.*, 2005). The sol-gel process can be described as the creation of an oxide network by progressive poly-condensation reactions of molecular precursors in a liquid medium. The surface ion-imprinted technique in combination with sol-gel process can easily synthesize a high cross-linking, better thermal stability and chemical stability material; on the other hand, the specific chemical functional groups inducted into the network structure can improve selectivity and specificity to template. Thus, this technology provides a new platform to prepare high performance ion-imprinted polymers (Li *et al.*, 2007; Elena *et al.*, 2005).

Nano-TiO₂ is a solid substrate with hydroxyl groups on its surface, which is allowed to react with glycidoxypropyltrimethoxysilane (GPTMS) (CH₂OCHCH₂O(CH₂)₃Si(OCH₃)₃) to form covalently-bound surface monolayers of the metal alkoxide (Gupta and Kumar, 2008) (Fig. 1). Nano-TiO₂ also has large surface area and excellent chemical stability. Because of those advantages, nano-TiO₂ was used as matrix in present study. Chitosan (CTS), poly (β-1,4)-2-amino-2-deoxy-D-glucopyranose, the free amido and hydroxyl function of chitosan give it a better ability to chelate ions of transition metals than other natural compounds (Rhazi, 2002). However, CTS with amido groups is linear polymer, causing CTS solubility in acidic conditions

* Corresponding author. E-mail: yys@ujs.edu.cn

jesc.ac.cn

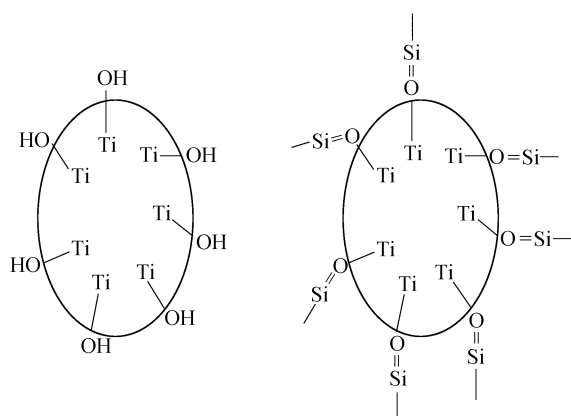


Fig. 1 Scheme of nano-TiO₂ (a) and nano-TiO₂ reacting with GPTMS (b).

commonly. Many researchers have studied its chemical modification, such as cross-linking (Viswanathan *et al.*, 2009), etherification (Qian *et al.*, 2008), grafting (Singh *et al.*, 2009). This work attempts to synthesize a Pb(II)-imprinted polymer based on the surface imprinting technique in combination with sol-gel process, which would resist the dissociation of CTS. Then the structural characteristics, adsorption and desorption behaviors towards Pb(II) in aqueous solution were described and discussed.

1 Materials and methods

1.1 Chemicals

Chitosan, degree of deacetylation more than 90% (Guoyao Chemical Reagents Corp., China) and GPTMS (Nanjing Shuguang Chemical Corp., China) were used. Nano-TiO₂ (Jiangsu Hehai Nano-materials Science and Technology Corp., China) was heated up at 110°C for 2 h to activate the surface. Standard stock solution of Pb(II) (1.0 mg/mL, Pb(NO₃)₂) was prepared using doubly distilled water (DDW). Standard working solutions were further diluted prior to use. All the chemicals used were in analytical grade.

1.2 Apparatus and measurement condition

The infrared spectra were recorded by a Nicolet NEXUS 470 FT-IR (Thermoelectric, USA) using KBr as background spectra. D-5005 powder X-ray diffractometer (XRD) (Siemens, Germany) was used with CuK_α radiation ($\lambda = 0.1541$ nm). Scanning electron microscopy (SEM) (S-4800, Hitachi High-Tech, Japan) was used after gold plating at 15 kV on the field emission SEM. VISTA-MPX Inductively coupled plasma atomic emission spectrometry (ICP-AES) (Varian Inc., USA) to determine heavy metals. The wavelengths selected were as follows: Cd 214.439 nm, Co 238.892 nm, Cr 267.716 nm, Cu 327.395 nm, Fe 238.204 nm, Hg 184.887 nm, Mg 279.553 nm, Mn 257.610 nm, Ni 231.604 nm, Zn 213.857 nm. The instrumental parameters were recommended by manufacturers. TAS-986 flame atomic absorption spectrophotometer (FAAS) (Shanghai Pudong Instruments,

China) was used and all measurements were carried out in an air/acetylene flame.

1.3 Synthesis Pb(II)-imprinted polymer

The following preparation procedures were modified from the literature (Li *et al.*, 2007). Chitosan (4.0 g) and Pb(NO₃)₂ (0.4 g) were dissolved in 160 mL of 0.1 mol/L HAc aqueous solution. After stirring for 1 h, 40 mL of GPTMS as both a crosslink and a silane coupling agent was added into the mixture. Then, the reaction was conducted for 4 h at 25°C with continuous stirring at 300 r/min, afterwards, the product was treated in an ultrasonic for 20 min to be dispersed equably. And then 20 g nano-TiO₂ was added under stirring vigorously. The wet product was allowed to evaporate at room temperature to complete the cross-linking reaction and gelation. The dry product was grinded and washed with DDW to remove non-bound Pb(II). The consequent polymer was filtered and treated with 3.0 mol/L HNO₃ to completely leach the coordinated Pb(II), and then washed several times with DDW and 0.1 mol/L NaOH to ensure the neutralization of hydrogen ion. The polymer was then filtered, dried at 50°C under vacuum, grinded and shifted with 100 meshes, resulting in the desired Pb(II)-imprinted polymer (IP). Non-imprinted polymer (NIP) was also prepared as a blank in parallel but without the addition of Pb(NO₃)₂.

1.4 Adsorption experiments

1.4.1 Pb(II) adsorption batch experiments

To study Pb(II) adsorption behavior under static conditions, the optimum conditions for adsorption were studied: effects of pH (1.0–9.0), kinetics of adsorption (30 min–10 h), adsorption isotherm (10–450 mg/L). The batch experiments were conducted as following steps: a solution containing 100 μ g Pb(II) was transferred into 50 mL colorimetric tube at a pH 5.0 (adjusted with 0.1 mol/L HCl and 0.1 mol/L NaOH) at room temperature, the volume was adjusted to 50 mL with DDW, and added 0.4 g IP (imprinted polymer). Then the mixture was shaken vigorously for 10 min, the adsorption time was maintained for 4.0 h. After centrifugation, the concentration of the Pb(II) in the residues solution was determined by FAAS. The adsorption rate (E , %) and absorption capacity (Q , mg/g) were calculated by Eqs. (1) and (2), respectively. The experimental steps could modify according to the actual situation.

$$E = \frac{C_0 - C}{C_0} \times 100\% \quad (1)$$

$$Q = \frac{(C_0 - C)V}{W} \quad (2)$$

where, C_0 (mg/L) and C (mg/L) are initial and equilibrated concentration of Pb(II). V (L) is solution volume and W (g) is the mass of Pb(II)-imprinted polymer.

1.4.2 Adsorption selectivity

To examine the adsorption selectivity of IP, recognition studies of the competitive metal ions were performed. The mix-metal-solution (100 μ g), including Pb(II), Cd(II),

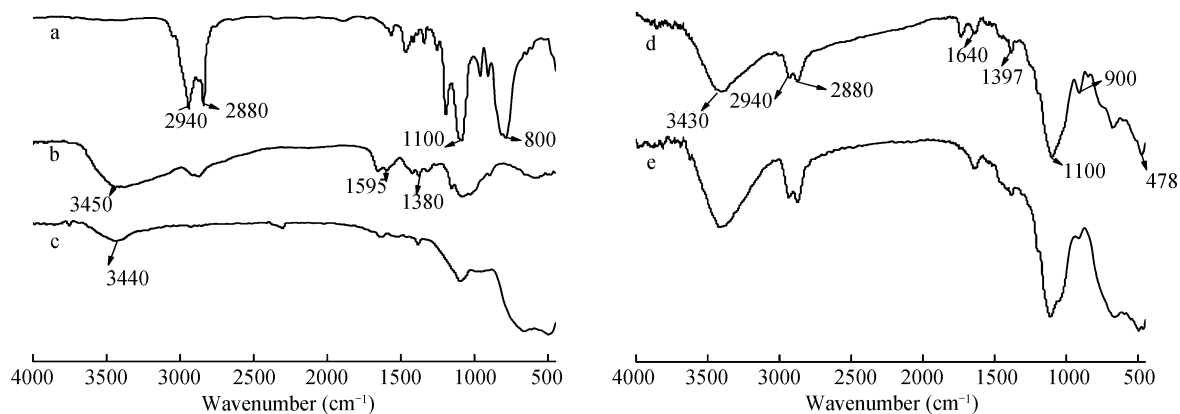


Fig. 2 Infrared spectra of GPTMS (line a), chitosan (CTS) (line b), nano-TiO₂ (line c), Pb(II)-imprinted polymer before leaching the Pb(II) (IPB) (line d), and Pb(II)-imprinted polymer (IP) (line e).

Co(II), Cr(III), Cu(II), Fe(III), Hg(II), Mg(II), Mn(II), Ni(II), Zn(II), was transferred into 50 mL colorimetric tube at pH 5.0, the volume was adjusted to 50 mL with DDW. Point four gram of imprinted and non-imprinted polymer were added, respectively, and the mixture solutions were shaken vigorously for 10 min. The adsorption time was 4.0 h. After centrifugation, the concentration of the metal ions (Pb(II), Cd(II), Co(II), Cr(III), Cu(II), Fe(III), Hg(II), Mg(II), Mn(II), Ni(II), Zn(II)) in the residues solution were determined. The distribution coefficient K_d (mL/g), selectivity coefficient k , and the relative selectivity coefficient k' were given in Eqs. (3)–(5).

$$K_d = \frac{(C_i - C_f)V}{C_f W} \quad (3)$$

$$k = \frac{K_{d_{pb}}}{K_{d_M}} \quad (4)$$

$$k' = \frac{k_{IP}}{k_{NIP}} \quad (5)$$

where, C_i and C_f represent the initial and equilibrated metal ions solution concentrations of the given metal ions, respectively; $K_{d_{pb}}$, K_{d_M} represent the distribution coefficient of Pb(II) and M (M = Cd(II), Co(II), Cr(III), Cu(II), Fe(III), Hg(II), Mg(II), Mn(II), Ni(II), Zn(II), respectively); k_{IP} , k_{NIP} represent the selectivity coefficient of IP and NIP, respectively.

1.5 Desorption experiments

Desorption of the adsorbed Pb(II) from the IP were also studied in a batch experiments: effects of HNO₃ concentration, HNO₃ volume and quiescent time on the recovery of Pb(II). The recovery rate (D , %) of Pb(II) in the desorption process was calculated by Eq. (6).

$$D = \frac{H_{de}}{H_{ad}} \times 100\% \quad (6)$$

where, H_{de} and H_{ad} are desorbed Pb(II) concentration in HNO₃ solution and by IP, respectively.

2 Results and discussion

2.1 Characterization

2.1.1 FT-IR results

As shown in Fig. 2, line b, the characteristic broad absorption bands at 3450 cm⁻¹ represented multi-overlapped absorption peaks of hydroxyl groups (O–H) and amido groups (N–H) stretching vibration, but these characteristic broad absorption bands shifted to 3430 cm⁻¹ and obviously become narrow (Fig. 2, line d). Comparing line b and line d: the characteristic feature of N–H at 1595 cm⁻¹ shifted to 1640 cm⁻¹ and C–N at 1380 cm⁻¹ shifted to 1397 cm⁻¹. Moreover, a new peak at 478 cm⁻¹ assigned to the Pb(II)–O appeared in Fig. 2, line d. It could be concluded that the –NH₂ and –OH groups in CTS are coordinate with Pb(II) simultaneity from the observed excursion of peaks. The results are in agreement with Ding *et al.* (2007).

The spectrum of GPTMS (Fig. 2, line a) shows the Si–O–Si peak at about 1100 cm⁻¹ and the peaks of 2960 cm⁻¹, 2874 cm⁻¹ were attributed to the stretching vibrations of –CH₃, all these peaks could be found but the intensity of the peaks was weakening in line d. The peak at 800 cm⁻¹ was assigned to epoxy group in GPTMS, which disappeared in line d. It can be concluded the GPTMS reacted with the amino group on CTS chains through its oxirane ring. The peak around 3440 cm⁻¹ was the Ti–OH on the surface of nano-TiO₂ (line c), which allowed to react with silantriol groups in GPTMS, as shown in Fig. 1. Hence, a new peak Si–O–Ti appeared in line d at about 900 cm⁻¹, and there was little change in the shape or shift from the observed excursion of line d and line e, presuming that 1 mol/L HNO₃ was intact in leached IP.

2.1.2 XRD patterns

Figure 3 shows the XRD patterns of the CTS, nano-TiO₂, and IP. There was a distinct crystalline peak around 20° in XRD patterns of the CTS. It probably because plenty of –NH₂ and –OH groups exist in the CTS structure, which can form strong intermolecular and intra-molecular hydrogen bonds, and thus the CTS molecules form crystalline regions easily. However, compared CTS with IP, the distinct crystalline peak around 20° disappeared. This is

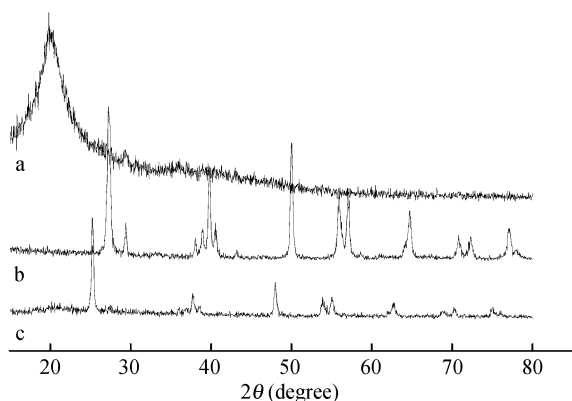


Fig. 3 X-ray spectra of CTS (line a), nano-TiO₂ (line b), IP (line c).

could be considered that Pb(II) was introduced into CTS main chains, that would destruct the intermolecular and intra-molecular hydrogen bonds and certain regularity of CTS (Duan *et al.*, 2008). By comparison with the standard pattern (JCPDS No 21-1272) of TiO₂ anatase phase, we could find nano-TiO₂ used in this work was anatase phase. The peaks in the nano-TiO₂ could be seen for IP but the intensity decreased greatly, which indicated that the Pb(II)-CTS coated onto nano-TiO₂, but did not destruct crystallinity and orderly structure of nano-TiO₂. Thus, Pb(II)-CTS coated just on the surface of nano-TiO₂ not in the interlayer via GPTMS as shown in Fig. 1.

2.1.3 Morphological structure

Figure 4 depicts the surface morphology of CTS, nano-TiO₂, IPB and IP at 1.00 μm. CTS was massive object, and nano-TiO₂ was small particles with loose structure. Unlike the SEM images of pure CTS and nano-TiO₂, the surface morphology of the IP was also composed by many small particles, and the small particles were adhesion instead of original loosely structured. It indicated that Pb(II)-CTS just coated onto nano-TiO₂ via GPTMS. The results were in agreement with the results of XRD. The morphology of IP was more unsmooth and uneven than IPB. Because Pb(II) was leached from the surface of organic-inorganic hybrid polymer, which would leave behind some cavities with selective to the template Pb(II) ions, and thus IP

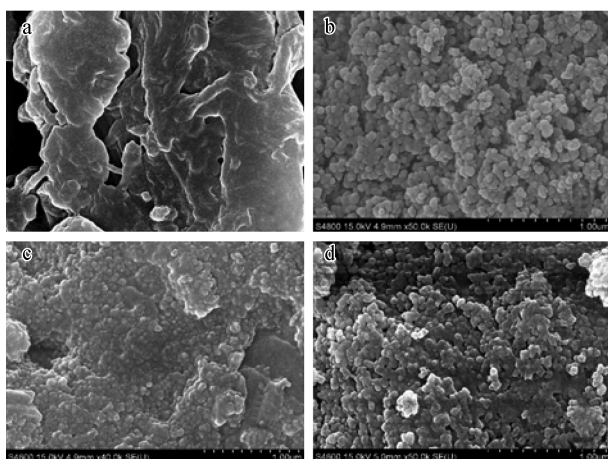


Fig. 4 SEM image of CTS (a), nano-TiO₂ (b), IPB (c), and IP (d).

possessed the capacity of selective adsorption Pb(II) ions.

2.2 Adsorption experiments

2.2.1 Effects of pH, amount of IP, and mixing time

The effect of pH on Pb(II) adsorption was studied at pH range 1.0–9.0. The results represented in Fig. 5 evident that the adsorption capacity of Pb(II) increased with solution pH. There was no adsorption at pH 1.0, and adsorption rate was low at pH 2.0. One reason is protonation (Varmaa *et al.*, 2004). An excess of hydrogen ions can compete effectively with Pb(II) for –NH₂ at low pH. Therefore, the strong acidic solution can be utilized for desorption Pb(II) from IP. Another reason is the increase of the activity of –NH₂ and –OH, due to the IP preparation in HAc solution. The adsorption rate exceeded 95% when pH was beyond 5.0. Thus, pH 5.0 was used as in the following experiments.

Experimental results indicated the optimal factors for IP amount of 0.4 g and shaking time of 10 min.

2.2.2 Adsorption kinetics

The kinetics curve of adsorption of Pb(II) on IP is illustrated in Fig. 6. The adsorption rate increased rapidly at first 3 h, then became slowly increased; and reached equilibration at the 4th hour. At initial fast adsorption stage, lots of binding sites were available for Pb(II) adsorp-

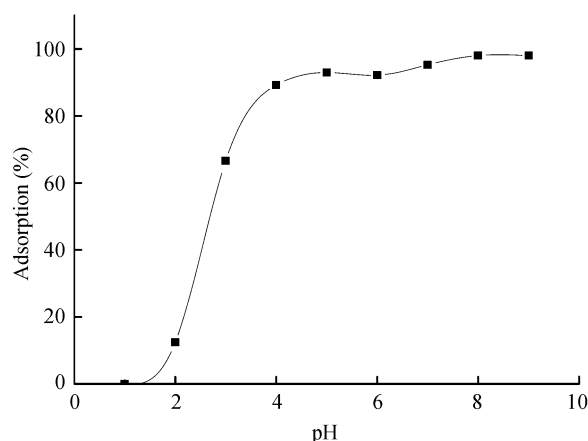


Fig. 5 Effect of pH on Pb(II) adsorption. Other conditions: IP 0.4 g; Pb(II) 2.0 mg/L; shaking time 10 min; adsorption time 4.0 h; temperature 25°C.

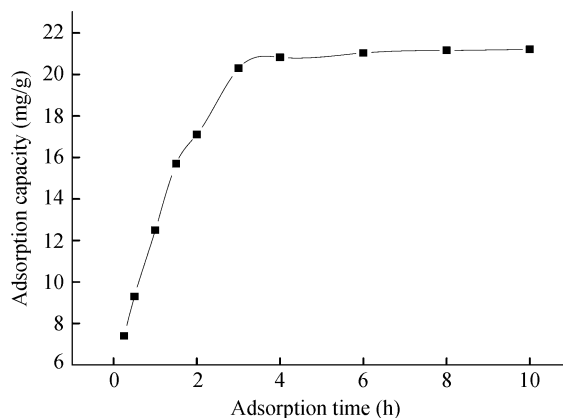


Fig. 6 Curve of kinetic adsorption. Other conditions: IP 0.4 g; pH 5.0; Pb(II) 300 mg/L; shaking time 10 min; temperature 25°C.

tion. Over period of time, the binding sites were filled with Pb(II), then adsorption equilibration was reached in a short time. The fast adsorption time also suggested that IP was suitable for pre-concentration of Pb(II) from large volume of solutions. To examine the underlying mechanism of the adsorption process, Lagergren pseudo first- (Eq. (7)) and second-order (Eq. (8)) kinetic model were applied.

$$\log(Q_{\max} - Q_t) = \log Q_{\max} - \frac{K_1 t}{2.303} \quad (7)$$

$$\frac{t}{Q_t} = \frac{1}{K_2 Q_{\max}^2} + \frac{t}{Q_t} \quad (8)$$

where, Q_{\max} (mg/g) and Q_t (mg/g) are the adsorption capacity at equilibrium and time t (h), respectively, K_1 (h^{-1}) and K_2 (mg/(g·h)) are pseudo first- and second-order rate constants of adsorption, respectively. Pseudo first-order model is rendered the rate of occupation of the adsorption sites to be proportional to the number of unoccupied sites; and pseudo second-order kinetic model is assumed the chemical reaction mechanisms (Iftikhar *et al.*, 2009), and that the adsorption rate is controlled by chemical adsorption through sharing or exchange of electrons between the adsorbent and adsorbent (Özacara *et al.*, 2008).

As shown in Table 1, the correlation coefficient for the pseudo second-order model was higher than first-order. Therefore, the adsorption behavior of Pb(II) on IP belonged to the second-order kinetic model and the adsorption process was a chemical process.

2.2.3 Adsorption isotherm

As shown in Fig. 7, adsorption capacity increased with initial concentration; after a certain concentration, the

Table 1 Comparison between Lagergren pseudo first- and second-order kinetic model

Experimental		Pseudo first-order	
Q_{\max} (mg/g)	K_1 (h^{-1})	Q_{\max} (mg/g)	R^2
21.21	0.0486	15.3	0.9705
Experimental		Pseudo second-order	
Q_{\max} (mg/g)	K_2 (mg/g/h)	Q_{\max} (mg/g)	R^2
21.21	0.9861	21.4	0.9897

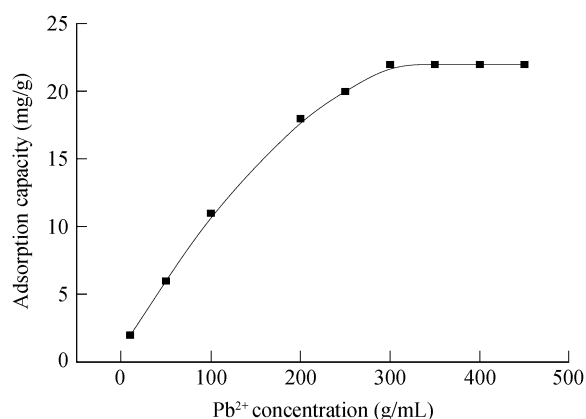


Fig. 7 Adsorption isotherms of Pb(II). Other conditions: IP 0.4 g; pH 5.0; shaking time 10 min; adsorption time 4.0 h; temperature 25°C.

adsorption reached saturation. It was likely owing to the less active sites being available at the end of the adsorption process. The adsorption isotherms curve was similar to the Langmuir adsorption isotherm (Eq. (9)).

$$\frac{C_e}{Q_e} = \frac{C_e}{Q_{\max}} + \frac{1}{K_L Q_{\max}} \quad (9)$$

where, C_e (mg/L) is the different initial concentration of Pb(II), Q_e (mg/g) is the adsorption capacity at the different initial concentration of Pb(II), and K_L (L/mg) is the adsorption-desorption equilibrium constant related to the binding energy. According to Langmuir model, adsorption was occurred uniformly on the active sites of the adsorbent. Once a sorbate occupied the site, no further adsorption could take place at this site (Bhatnagar and Jain, 2005). Thus, experimental data were fitted to Langmuir adsorption isotherm model, as shown in Table 2. The adsorption process of Pb(II) onto IP could be considered the monolayer adsorption.

For predicting the favorability of an adsorption system, the Langmuir equation can also be expressed in terms of a dimensionless separation factor R_L (Eq. (10)) (Shen *et al.*, 2009; Huang *et al.*, 2007).

$$R_L = \frac{1}{(1 + C_e K_L)} \quad (10)$$

where, R_L indicates the favorability and the capacity of the adsorbent/adsorbate system. When $0 < R_L < 1$, it represents good adsorption. As shown in Table 3, the present adsorption systems were favorable and the adsorption of Pb(II) was more favorable at higher initial Pb(II) concentrations than at lower concentrations.

2.2.4 Adsorption selectivity

To investigate the selectivity of IP, adsorption capacities of IP and NIP in mix-solution, including Pb(II), Cd(II), Co(II), Cr(III), Cu(II), Fe (III), Hg(II), Mg(II), Mn(II), Ni(II), and Zn(II), were examined, respectively. Obviously, IP had the highest adsorption rate for Pb(II) among studied metal ions (Fig. 8). A comparison of the adsorption rate between IP and NIP suggested that the IP had a specific selectivity to Pb(II) but non-specific selectivity to the other metal ions.

The sizes of Co(II), Cr(III), Fe(III), Mg(II), Mn(II), Ni(II), Zn(II) were smaller or larger than Pb(II). The

Table 2 Langmuir adsorption isotherm model for Pb(II) adsorption onto IP

Langmuir			Experimental
Q_{\max} (mg/g)	K_L (L/mg)	R^2	Q_{\max} (mg/g)
32.15	0.00577	0.9691	22.7

Table 3 Separation factor R_L for Pb(II) adsorption onto IP

C_e (mg/L)	10	50	100	200	250
R_L	0.9454	0.7794	0.6369	0.4673	0.4124
C_e (mg/L)	300	350	400	450	
R_L	0.3690	0.3339	0.3049	0.2779	

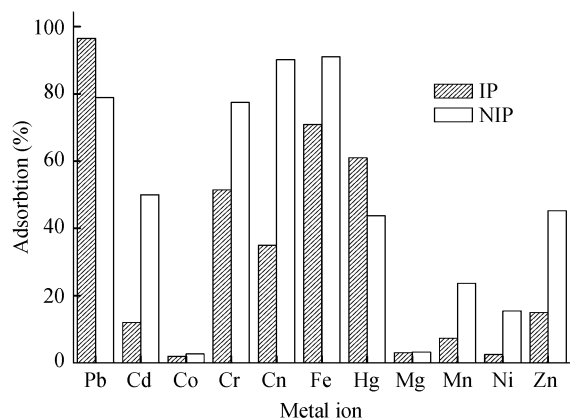


Fig. 8 Competitive adsorption of metal ions onto IP and NIP. Other conditions: IP: 0.4 g; NIP: 0.4 g; pH 5.0; 2.0 mg/L of mix-solution; shaking time 10 min; adsorption time 4.0 h; temperature 25°C.

adsorption rates of IP for these ions were lower than NIP, due to the shape of cavities, which matched with the structure of Pb(II). On the other hand, Cd(II), Cu(II), Hg(II) had the similar sizes with Pb(II), the adsorption rate of IP for these ions were also lower than NIP. It should be the coordination-geometry selectivity, because IP could provide ligand groups arranged in a suitable way required for coordination of Pd(II) only (Fang *et al.*, 2005). Consequently, hole-size and coordination-geometry selectivity were also the reasons of Pb(II) selection from mix-solution.

As shown in Table 4, K_d of Pb(II) adsorption by IP was significantly larger in comparison with Pb(II) adsorption by NIP and other metal ions adsorption by IP. NIP has low k values due to NIP without special size of the cavity and the specific binding sites containing functional groups in a predetermined orientation. It demonstrated that IP synthesized for the Pb(II) adsorption had a higher selectivity.

2.3 Desorption

According to the batch test of pH effect, it can be concluded that adsorbed Pb(II) can be released in acidic solution. HNO₃ was chosen as eluant. The concentration of HNO₃ for desorption must be optimized, because a lower concentration of HNO₃ may be not strong enough

Table 4 Effect of imprinting on selectivity

	IP		NIP		k'
	k_d (mL/g)	k	k_d (mL/g)	k	
Pb(II)	1723		235		
Cd(II)	9	191	62.5	4	47.7
Co(II)	3	574	3.2	73	8
Cr(III)	66	26	250	0.94	28
Cu(II)	34	50	562.5	0.42	119
Fe(III)	187	9	667	0.35	26
Hg(II)	116	15	51	4.6	3.2
Mg(II)	4	431	4	59	7
Mn(II)	6	287	21	11	26
Ni(II)	3.5	492	11	21	23
Zn(II)	11	157	114	2	78.5

k_d : distribution coefficient; k : selectivity coefficient; k' : relative selectivity coefficient.

to protonate $-NH_2$. Therefore, volume quantity of HNO₃ is an important factor. The effects of HNO₃ concentration, volume, shaken time and quiescent time on Pb(II) recovery were evaluated. As shown in Table 5, the recovery rate of Pb(II) increased gradually with the rise of concentration and volume of HNO₃. In order to make desorption completely and integrated actual conditions, we should select the optimal desorption conditions as: 10 mL of 1 mol/L HNO₃ and quiescent time of 2.0 h.

2.4 Regeneration

After adsorption-desorption, the IP was regenerated with 3 mol/L HNO₃, then was soaked for 24 h, neutralized, washed with DDW and dried under vacuum, and then to adsorb Pb(II) again. After four adsorption-desorption-regeneration cycles with the same adsorbent in batch experiments, the adsorption rate of IP for Pb(II) still exceeded 90%. It could be concluded that IP can be used many times without decreasing their adsorption capacities significantly.

2.5 Effect of interfering ion

The effect of the interference ion is a main problem on the FAAS determination of metal ions (Tuzena *et al.*, 2008). Different amounts of cations and anions were added to the test solution containing 100 µg Pb(II), respectively, and the other steps were similar to the procedures described in Section 2.4.1. The results given in Table 6 show that the effects of other metal ions at given concentrations were negligible. It implied that IP had a potential application in the determination of water samples which contained diverse ions.

2.6 Recovery rate from water samples

A certain amount of well-water (collected residential areas near Yangtze River) was acidified by HCl (1:1, V/V), heated to concentrate, cool down and filtered. The filtrate was analyzed after preparation. The adsorption-desorption

Table 5 Effects of HNO₃ concentration, volume and quiescent time on the desorption of Pb(II)

Conc. (mol/L)	Recovery (%)	Volume (mL)	Recovery (%)	Quiescent time (min)	Recovery (%)
0.1	82.3	5	73.2	0.5	90.2
0.5	90.5	10	91.5	1.0	92.3
1	94.3	15	92.8	2.0	94.3
2	100.1	20	94.2	3.0	96.5

Table 6 Effect of interfering ions on the recovery of Pb(II)

Ion amount (µg)	Recovery (%)	Ion amount (µg)	Recovery (%)		
K(I)	7000	94.5	Cd(II)	2000	93.3
Na(I)	6000	96.1	Cl ⁻	9000	97.8
Ca(II)	6000	95.8	Cr(III)	3000	92.4
Mg(II)	6000	93.9	Hg(II)	2000	92.1
Al(III)	5000	92.7	Mn(II)	3000	92.3
Fe(III)	3000	91.5	NO ₃ ⁻	7000	95.5
Zn(II)	3000	96.0	SiO ₃ ²⁻	1000	86.5
Cu(II)	3000	95.8	WO ₄ ²⁻	4000	90.5

procedures were applied to determine the recovery rate after adding different concentrations of Pb(II) in water samples. The results are described in Table 7, in which all recoveries were in the acceptable level and gave a high precision. The results demonstrated the applicability of the IP can separate and enrich Pb(II) from water samples. The precision of the procedure is 4.1% (Pb(II): 5 µg/mL, $n = 11$). According to the definition of IUPAC to the detection limit, this method detection limit was 0.047 µg/mL.

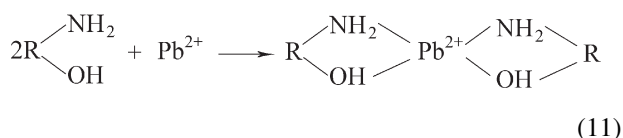
Table 7 Analytical results of recovery rate in water samples ($n = 3$)

Pb(II) dosage (µg)	Recovery (%)	RSD (%)	Average recovery (%)
100	98	2.3	94
200	95	1.3	
300	89	3.6	
400	93	2.8	

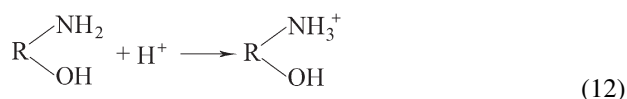
2.7 Adsorption mechanism

As described in Section 2.2.3, Pb(II) adsorption onto IP can be fitted well by the pseudo second-order kinetic model. And the pseudo second-order kinetic model is assumed the chemical reaction mechanisms, which include ion-exchange, adsorption, chemisorption and chelation.

First, nitrogen and oxygen atoms of IP have lone pairs of electrons that can bind Pb(II) through an electron pair sharing to form a complex. The divalent heavy Pb(II) attaches two adjacent amino groups and two hydroxyl groups which could donate two pairs of electrons to metal ions, forming four coordination number compounds (Li *et al.*, 2003). In the present study, Pb(II) may be adsorbed onto IP through chelation mechanisms. The reaction may be represented as Reaction (11).



Second, the influences of pH and Pb(II) initial concentration on the adsorption rate suggests that there is a competitive adsorption of Pb(II) and H^+ to the nitrogen atom (Li and Bai, 2002). At low pH, the nitrogen atom would be protonated.



where, R is all other components except $-\text{NH}_2$ and $-\text{OH}$ in the IP. Used 1 mol/L HNO_3 for desorption, the Reaction (12) would be take place through a competitive adsorption of H^+ over Pb^{2+} to the nitrogen atom, which may be considered as an ion exchange mechanism. Therefore, Pb(II) may release out from IP by ion exchange mechanism. The reaction may be represented according to Reaction (13).

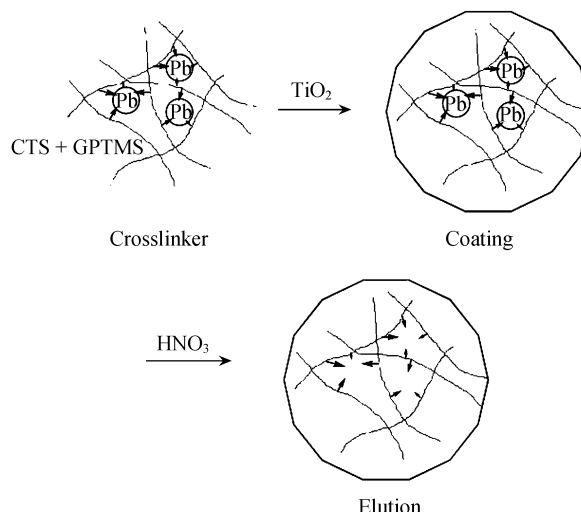
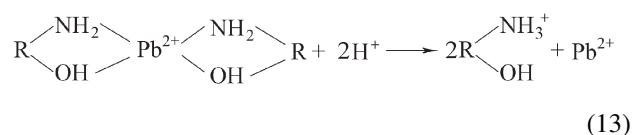


Fig. 9 Schematic representation of ion imprinting.



Third, IP is like a tailored material (Rao *et al.*, 2004) (Fig. 9), which copies the model of Pb(II) to tailor. Other metal ions can chelation with nitrogen and oxygen atoms of IP, but they did not fit the tailored materials (viz IP). Therefore, IP has a selectivity only to Pb(II). According to selectivity experiment, the selectivity mainly was controlled by the shape of cavities (the size of the metal ions) and coordination-geometry.

3 Conclusions

The surface ion-imprinted technology in combination with sol-gel method was applied successfully to synthesize Pb(II)-imprinted polymer. The optimal adsorption and desorption conditions of Pb(II)-IP system were investigated. The kinetics of adsorption was fitted the pseudo second-order model, implying the adsorption behavior of Pb(II) on IP was a chemical process. The adsorption isotherm was described by the Langmuir model, and the present adsorption systems were favorable ($0 < R_L < 1$).

The Pb(II)-imprinted polymer showed a higher selectivity for targeted Pb(II). The recognition function of the Pb(II)-imprinted polymer was attributed to the shape of cavities and coordination-geometry. The adsorption/desorption mechanism may be chelation/ion exchange.

The Pb(II)-imprinted polymer has a superior reusability and stability. The preconcentration and recovery of Pb(II) has also been investigated from water samples. The average recovery of Pb(II) was 95%.

Acknowledgments

This work was supported by the National Natural Science Foundation of China (No. 20877036).

References

- Anthemidis A N, 2008. Automatic sequential injection liquid-liquid micro-extraction system for on-line flame atomic absorption spectrometric determination of trace metal in watersamples. *Talanta*, 77(2): 541–545.
- Birlik E, Ersöz A, Ackkalp E, Denizli A, Say R, 2007. Cr(III)-imprinted polymeric beads: Sorption and preconcentration studies. *Journal Hazardous Materials*, 140(1-2): 110–116.
- Baghel A, Boopathi M, Singh B, Pandey P, Mahato T H, Gutch P K *et al.*, 2007. Synthesis and characterization of metal ion imprinted nano-porous polymer for the selective recognition of copper. *Biosensors & Bioelectronics*, 22(12): 3326–3334.
- Bhatnagar A, Jain A K, 2005. A comparative adsorption study with different industrial wastes as adsorbents for the removal of cationic dyes from water. *Journal Colloid and Interface Science*, 281(1): 49–55.
- Ding C M, Yue W J, Su Y, Li G Y, Guo L, Chen L, 2007. Preparation and spectral analysis of coordination compounds of chitosan with Ce(III), Zr(IV), Pb(II) and Cd(II). *Spectroscopy and Spectral Analysis*, 27: 1185–1187.
- Duan W G, Chen C H, Jiang L b, Li G H, 2008. Preparation and characterization of the graft copolymer of chitosan with poly[rosin-(2-acryloyloxy)ethyl ester]. *Carbohydrate Polymers*, 73(4): 582–586.
- Elena M, García D, Laíño R B, 2005. Molecular imprinting in sol-gel materials: Recent developments and applications. *Microchimica Acta*, 149(1-2): 19–36.
- Fang G Z, Tan J, Yan X P, 2005. An ion-imprinted functionalized silica gel sorbent prepared by a surface imprinting technique combined with a sol-gel process for selective solid-phase extraction of cadmium(II). *Analytical Chemistry*, 77(6): 1734–1739.
- Gupta R, Kumar A, 2008. Molecular imprinting in sol-gel matrix. *Biotechnology Advances*, 26(6): 533–547.
- Huanga J H, Liua Y F, Jina Q Z, Wanga X G, Yang J, 2007. Adsorption studies of a water soluble dye, Reactive Red MF-3B, using sonication-surfactant-modified attapulgite clay. *Journal of Hazardous Materials*, 143(1-2): 541–546.
- Iftikhar A R, Bhatti H N, Hanifa M A, Nadeem R, 2009. Kinetic and thermodynamic aspects of Cu(II) and Cr(III) removal from aqueous solutions using rose waste biomass. *Journal of Hazardous Materials*, 161(2-3): 941–947.
- Li J Y, Shukla S S, Dorris K L, Shukla A, Margrave J L, 2003. Adsorption of chromium from aqueous solutions by maple sawdust. *Journal of Hazardous Materials*, 100(1-3): 53–63.
- Li J, Bai R B, 2002. Mechanisms of lead adsorption on chitosan/PVA hydrogel beads. *Langmuir*, 18(25): 9765–9770.
- Li F, Jiang H Q, Zhang S S, 2007. An ion-imprinted silica-supported organic-inorganic hybrid sorbent prepared by a surface imprinting technique combined with a polysaccharide incorporated sol-gel process for selective separation of cadmium(II) from aqueous solution. *Talanta*, 71(4): 1487–1493.
- Prasad K, Gopikrishna P, Kala R, Rao T P, Naidu G R K, 2006. Solid phase extraction vis-à-vis coprecipitation preconcentration of cadmium and lead from soils onto 5,7-dibromoquinoline-8-ol embedded benzophenone and determination by FAAS. *Talanta*, 69(4): 938–945.
- Qian T S, Yao D X, Zhou F M, 2008. Antioxidant activity of N-carboxymethyl chitosan oligosaccharides. *Bioorganic & Medicinal Chemistry Letters*, 18(21): 5774–5776.
- Rhazi M, Desbrieres J, Tolaimate A, Rinaudo M, Vottero P, Alagui A *et al.*, 2002. Influence of the nature of the metal ions on the complexation with chitosan. Application to the treatment of liquid waste. *European Polymer Journal*, 38(8): 1523–1530.
- Rao T P, Daniel S, Gladis J M, 2004. Tailored materials for preconcentration or separation of metals by ion-imprinted polymers for solid-phase extraction (IIP-SPE). *Trends in Analytical Chemistry*, 23(1): 28–35.
- Singh V, Sharma A K, Tripathi D N, Sangh R, 2009. Poly(methylmethacrylate) grafted chitosan: An efficient adsorbent for anionic azo-dyes. *Journal of Hazardous Materials*, 161(2-3): 955–966.
- Shen W, Chen S Y, Shi S K, Xiang X L, Hu W L, Wang H P, 2009. Adsorption of Cu(II) and Pb(II) onto diethylenetriamine-bacterial cellulose. *Carbohydrate Polymers*, 75(1): 110–114.
- Tuzena M, Citaka D, Soylak M, 2008. 5-Chloro-2-hydroxyaniline-copper(II) coprecipitation system for preconcentration and separation of lead(II) and chromium(III) at trace level. *Journal of Hazardous Materials*, 158(1): 137–141.
- Viswanathan N, Sundaram C S, Meenakshi S, 2009. Sorption behaviour of fluoride on carboxylated cross-linked chitosan beads. *Colloids and Surface B: Biointerfaces*, 68(1): 48–54.
- Varmaa A J, Deshpandea S V, Kennedy J F, 2004. Metal complexation by chitosan and its derivatives: a review. *Carbohydrate Polymers*, 55(1): 77–93.
- Yilmaz E, Ramstrom O, Moller P, Sanchez D, Mosbach K, 2002. A facile method for preparing molecularly imprinted polymer spheres using spherical silica templates. *Journal of Materials Chemistry*, 12(5): 1577–1581.
- Yang H H, Zhang S Q, Tan F, Zhuang Z X, Wang X R, 2005. Surface molecularly imprinted nanowires for biorecognition. *Journal of the American Chemical Society*, 127(5): 1378–1379.
- Özacara M, Sengilb I A, Türkmenler H, 2008. Equilibrium and kinetic data, and adsorption mechanism for adsorption of lead onto valonia tannin resin. *Chemical Engineering Journal*, 143(1-3): 32–42.